Journal of Solid State Chemistry 201 (2013) 229–236

Contents lists available at SciVerse ScienceDirect

Journal of Solid State Chemistry

journal homepage: www.elsevier.com/locate/jssc

The site-selective excitation and the dynamical electron–lattice interaction on the luminescence of YBO_3: Sb^{3+}

Lei Chen [a,f,*], An-Qi Luo [a], Yao Zhang [a], Xin-Hui Chen [a], Hao Liu [a], Yang Jiang [a,1], Shi-Fu Chen [b,2], Kuo-Ju Chen [c], Hao-Chung Kuo [c], Ye Tao [d], Guo-Bin Zhang [e]

[a] School of Materials Science and Engineering, Hefei University of Technology, Hefei 230009, China
[b] Department of Chemistry, Huaibei Normal University, Huaibei 235000, China
[c] Institute of High Energy Physics, Chinese Academy of Sciences, Beijing 100039, China
[d] Department of Photonic & Institute of Electro-Optical Engineering, National Chiao Tung University, Hsinchu 30010, Taiwan
[e] National Synchrotron Radiation Laboratory, University of Science and Technology of China, Hefei 230026, China
[f] Semiconductor and Optoelectronic Technology Engineering Research Center of Anhui Province, Wuhu 241000, China

ARTICLE INFO

Article history:
Received 19 December 2012
Received in revised form
19 February 2013
Accepted 24 February 2013
Available online 7 March 2013

Keywords:
Phosphor
Luminescence
Site-selective excitation
Electron–lattice interaction
YBO_3: Sb^{3+}

ABSTRACT

The phosphor of YBO_3: Sb^{3+} was synthesized by solid state reaction. Its crystal structure was examined by using X-ray diffraction analysis. The morphology and particle size were characterized with a scanning electron microscopy. The properties of YBO_3: Sb^{3+} luminescence was systematically studied by exciting borate host, the $^1P_1$ and $^3P_1$ levels of Sb^{3+} at the C_i and C_1 sites with 168, 203, 218, 252 and 262 nm, respectively, measured on the synchrotron radiation instruments. The different configurations of emission spectra excited with variant wavelengths show the character of wavelength-selective excitation, which was attributed to different occupations of the Sb^{3+} site in the YBO_3 crystal lattice. Moreover, strong electron–lattice interaction (i.e., the Jahn–Teller effect) between Sb^{3+} and YBO_3 host was discriminated by comparing low temperature and room temperature spectra. The site-selective luminescence was confirmed by YBO_3 activated with multiple Sb^{3+} concentrations. The spectral assignment was verified with fluorescence lifetime achieved by using the Time-Correlated Single-Photon Counting method.

1. Introduction

The luminescence of Sb^{3+}, which originates from ns^2–$nsnp$ transition for its ns^2 configuration, has a large cross section to capture excitation energy and then transfer to other activators. Thus, Sb^{3+} was promisingly served as either an activator or a sensitizer in phosphors [1–5]. Typically, Sb^{3+} was utilized as a sensitizer for the activator of Mn^{2+} in warm white phosphor of $3Ca_3(PO_4)_2 \cdot Ca(F,Cl)_2$:$Sb^{3+}$,$Mn^{2+}$ for traditional fluorescent lamp [4,5]. Accordingly, the spectroscopic properties of Sb^{3+} ion have attracted wide attention [6–13].

Although several theoretical and experimental researches had addressed the luminescent properties of Sb^{3+}, there were still some controversies over the assignment of Sb^{3+} excited states and the case of electron transitions [6–13]. For example, the three excitation bands of $Cs_2NaScCl_6$ which consists of a doublet around 275,000 cm^{-1}, a weaker band at about 31,600 cm^{-1} and a triplet around 34,700 cm^{-1}, were attributed to $^1S_0 \rightarrow {}^3P_1$, $^1S_0 \rightarrow {}^3P_2$ and $^1S_0 \rightarrow {}^1P_1$ transitions, respectively; and the corresponding singlet emission band was designed to $^3P_1 \rightarrow {}^1S_0$ transition [6]. Three excitation bands with maxima at about 250 nm, 230 nm (weak) and 205 nm were attributed to $^1S_0 \rightarrow {}^3P_1$, $^1S_0 \rightarrow {}^3P_2$ and $^1S_0 \rightarrow {}^1P_1$ transitions, while the emission bands peaked at 415 nm and 520 nm were attributed to the isolated Sb^{3+} and the clusters of Sb^{3+} in oxychloride phase of LaOCl, respectively [7]. As for $Ln(PO_3)_3$:Sb^{3+} (Ln=Sc, Lu, Gd), the doublet shape of the excitation spectrum of $Ln(PO_3)_3$:Sb^{3+} (Ln=Sc, Lu, Gd) was attributed to the influence of different sites (not to the Jahn–Teller effect), but that was ascribed to the superposition of the Jahn–Teller effect and sites effect in $Y(PO_3)_3$: Sb^{3+} [8].

Thanks to the recent development of 3-dimension television (3D TV) technology, the research on plasma display panel (PDP) catched the eye once again. A phosphor which could emit efficiently under vacuum ultraviolet (VUV, 100–200 nm) excitation was desired for improvement of PDPs efficiency. Moreover, a material that can convert 172 nm photons into ultraviolet or visible light was still desired for space particle detector for a long

* Corresponding author at: School of Materials Science and Engineering, Hefei University of Technology, Hefei 230009, China. Fax: +86 551 62901362.
E-mail addresses: shanggan2009@qq.com (L. Chen), apjiang@hfut.edu.cn (Y. Jiang), chshifu@chnu.edu.cn (S.-F. Chen).
[1] Fax: +86 551 62904358.
[2] Fax: +86 561 3806611.

0022-4596/$ - see front matter © 2013 Elsevier Inc. All rights reserved.
http://dx.doi.org/10.1016/j.jssc.2013.02.034

time, because the vacuum ultraviolet photomultiplier tube that was used to detect the 172 nm photons radiated by xenon discharge was very costly [14–16]. YBO_3 was a promising host for these applications due to its high UV (200–400 nm) transparency, strong absorption in the VUV wavelength range, exceptional optical damage threshold, easy synthesis, good maintenance, and well chemical inert properties [17–19].

Earlier in 1986, the luminescence of YBO_3: Sb^{3+} had been investigated by Oomen et al. [20]. In his research, one broad emission band which consisted of two nearly overlapping bands and each with its own excitation spectrum was observed, but the short-limit wavelength of excitation spectrum was measured only to 250 nm [20]. The experiments implemented under UV excitation were unable to reveal the full-scale properties of Sb^{3+}, because the host absorption band of YBO_3 and the $^1S_0 \rightarrow {}^1P_1$ transition of Sb^{3+} may lie beyond the spectral range of UV spectrometer. Correspondingly, some interesting phenomena or some important mechanisms were ignored. For example, the strongly dynamical electron–lattice interaction between host and activator which had been observed in YPO_4 [12] and Ca(S, Se) [21] and Cs_2NaMCl_6 (M=Sc, Y, La) [9], but it was not observed in YBO_3 previously reported by Oomen et al. [20]. To obtain highly efficient luminescence, nevertheless, the effect of instantaneous polarization field which was caused by the thermal dynamical vibration of cations and polyanion groups must be suppressed. For which, the mechanism must be identified first of all. So, it is necessary to investigate the properties of Sb^{3+} luminescence under VUV excitation. For these reasons, the photoluminescence of YBO_3: Sb^{3+} was further investigated in this work. The phosphor of YBO_3: Sb^{3+} was synthesized with solid-state reaction method and its micro-structure was examined by using X-ray diffraction analysis and scanning electron microscopy. The luminescence properties were characterized by using a fluorescence spectrometer and the synchrotron radiation instruments. Besides the site-selective luminescence of Sb^{3+} in YBO_3, the dynamical electron–lattice interaction between the activator of Sb^{3+} and the host of YBO_3 was confirmed.

2. Experimental

Samples were synthesized from Y_2O_3 (99.9%), Sb_2O_3 (99.9%) and H_3BO_3 (99.5%) by a solid state reaction as following processes. Firstly, a stoichiometric mixture of the raw materials with a 5% excess H_3BO_3 was thoroughly grounded and pre-fired at 800 °C for 120 min. Then, the power was grounded for a next time and sintered at 1150 °C for 240 min in the air. After cooled down to room temperature with finance, the fired product was grounded and washed with 80–100 °C de-ionized water for several times to remove excess B_2O_3. Finally, it was dried at 120 °C.

Crystal structure of sample was identified by using an X-ray diffraction (XRD, Rigaku, D/Max-rB) with Cu$K\alpha$ (λ=1.5408 Å) radiation. Particles size and morphology were characterized with a scanning electron microscope (SEM, JEOL, JSM-6490LV). The UV excitation and emission spectra were collected with a Hitachi F-4500 fluorescence spectrometer at room temperature. The room-temperature VUV/UV excitation and emission spectra were measured at the National Synchrotron Radiation Laboratory (NSRL) VUV spectroscopy workstation on the U24 beam line. The workstation is equipped with a Seya–Namioka excitation monochromator (1200 g/mm, 100–400 nm), an ACS-257 emission monochromator (1200 g/mm, 200–700 nm), and a Hamamatsu H8259-01 photomultiplier detector. The cryogenic VUV/UV excitation and emission spectra were recorded at the VUV spectrum experimental station on the beam line 4B8 of Beijing Synchrotron Radiation Facilities (BSRF). A cryostat head with sample holder was installed on a manipulator (MB1504; McAllister), used to adjust, optimize and restore the position of the sample. The fluorescence was collected and focused by two lenses and projected onto the entrance slit of a fluorescence monochromator (SP308, Acton), which holds three gratings covering the range from 190 to 1700 nm with spectral resolution of 0.2 nm. The fluorescence signals were detected by the photon counting heads (H6241, Hamamatsu), and the output pulses were input into the counter module (974, ORTEC). More parameters for this workstation please refer to Ref. [22]. During measurement, the electron energy in storage ring was kept at 800 MeV for NSRL and 2.5 GeV for BSRF. The beam current was in the range of 150–250 mA for NSRL and 235–265 mA for BSRF, respectively. The pressure in sample chamber was kept about 10^{-3} Pa. All excitation spectra were calibrated with the sodium salicylate. The lifetime of luminescence was measured with the single photon account method by using the FLUOROLOG-3-TAU Time-Correlated Single-Photon Counting Spectrofluorometer.

3. Results

Although numerous studies have been carried out about the crystal structure of YBO_3, there were a larger amount of controversies over them [23–33]. One recent revision was carried out by Chadeyron by adopting single-crystal techniques combining with ^{11}B nuclear magnetic resonance (NMR) and infrared spectroscopy (IR) studies [23]. Chadeyron attributed the crystal structure of the YBO_3 to the space group $P63/m$ [23]. As for the method of X-ray diffraction, however, it was not easy to identify the space group. Recently, Lin's study, using neutron diffraction, shows the space group $C2/c$ [24]. Nevertheless, either Chadeyron's research or Lin's work, they both approbated that there are two kinds of Y^{3+} site and Y^{3+} is 8-coordinated with oxygen atoms. Later, Tanner used the low-temperature high-resolution emission spectroscopy to probe the local site symmetries of Eu^{3+} ions accommodated on the Y^{3+} sites in YBO_3: Eu^{3+} (0.5 at%) [25]. The use of point group selection rules enabled a consistent spectral interpretation by envisaging distinct C_i and C_1 symmetry Eu^{3+} sites, in accordance with the neutron diffraction study of Lin's [24,25].

Fig. 1 presents the XRD pattern of the as-prepared sample of $Y_{0.92}BO_3$: $Sb^{3+}_{0.08}$. By comparing the XRD patterns with JCPDS: 88-0356 (the $P63/m$ space group) revised by Chadeyron et al. [23] in 1997 by using the x-ray diffraction of the YBO_3 single crystal and

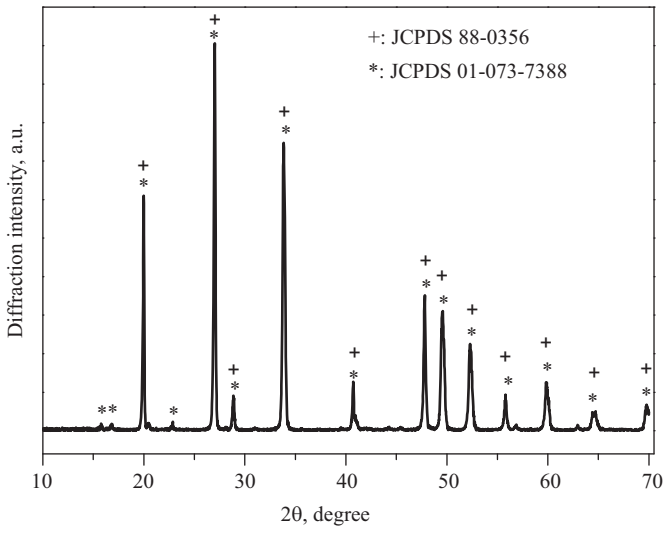

Fig. 1. The XRD pattern of $(Y_{0.92}Sb_{0.08})BO_3$.

JCPDS: 01-073-7388 (the $C2/c$ space group) resolved by Lin et al. [24] in 2004 using neutron diffraction method, the diffraction peaks shown in Fig. 1 is more consistent with the later one. Lin's work indicated that the low-temperature YBO_3 crystallizes in a C-centered monoclinic cell with $C2/c$ space symmetry, the unit cell parameters being $a=11.3138(3)$ Å, $b=6.5403(2)$ Å, $c=9.5499(2)$ Å, and $\beta=112.902(1)^\circ$ [24]. Fig. 2 shows that phosphor particles have a potato-like profile with average size about 2–5 μm. Figs. 1 and 2 demonstrated that the sample of YBO_3: Sb^{3+} was well synthesized here.

Fig. 3 presents the emission spectra of $(Y_{0.92}Sb_{0.08})BO_3$ by exciting with 230, 258 and 270 nm at room temperature measured with a Hitachi F-4500 spectrophotometer, in which one broad emission band with peak around 410 nm is observed. Typically, the asymmetric configuration of the emission spectra indicates that the broadband consists of more than one peak. This conclusion is demonstrated with cryogenic spectra in Fig. 4. Fig. 4 plots the emission spectra by exciting with 168, 203, 218, 225, 252, and 262 nm test on the beam line of 4B8 of BSRF synchrotron instrument at 14 K. The asymmetric configuration is observed in all spectra, but the emission spectrum excited with 262 nm

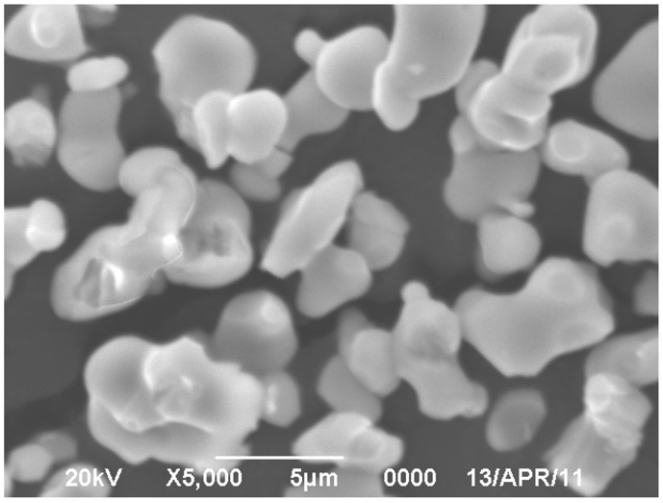

Fig. 2. Particle size and morphology of the YBO_3: Sb^{3+} phosphor.

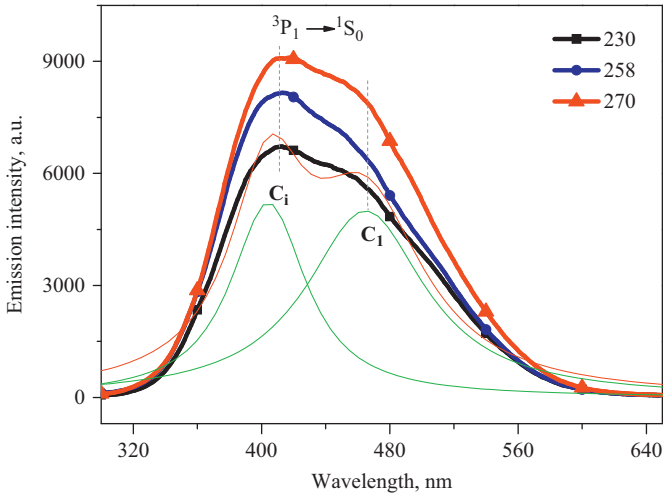

Fig. 3. The emission spectra of $(Y_{0.92}Sb_{0.08})BO_3$ by exciting with 230, 258 and 270 nm collected with the Hitachi F-4500 spectrophotometer at room temperature.

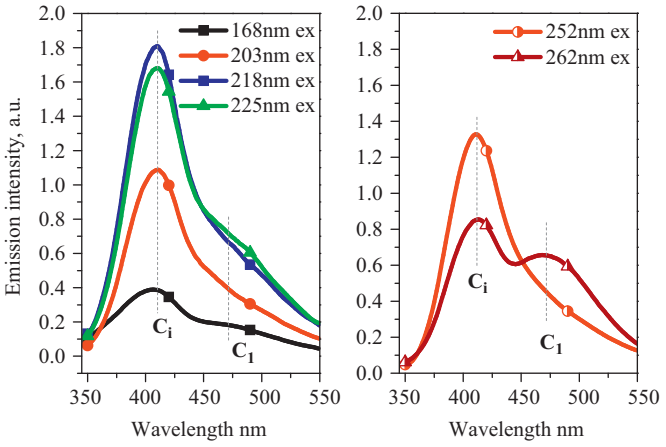

Fig. 4. The emission spectra of $(Y_{0.92}Sb_{0.08})BO_3$ by exciting with 168, 203, 218, 225, 252 and 262 nm measured on the BSRF synchrotron instrument at 14 K.

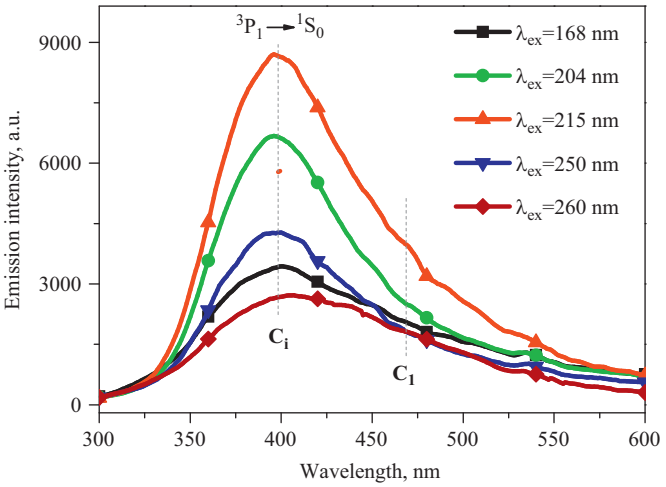

Fig. 5. The emission spectra of $(Y_{0.92}Sb_{0.08})BO_3$ by exciting with 168, 204, 215, 250 and 260 nm test on the NSRL synchrotron instrument at room temperature.

clearly shows that the emission band comprises of two peaks: one at about 410 nm and the other at approximate 470 nm.

Fig. 5 presents the emission spectra of $(Y_{0.92}Sb_{0.08})BO_3$ under 168, 204, 215, 250, and 260 nm excitation measured on the U24 beam line of the NSRL synchrotron instrument at room temperature. Although the emission spectra in Fig. 5 differ a little from those in Fig. 3, the asymmetric configuration is the common character of them and they are all measured at room temperature. One possible explanation for this difference is caused by the resolution or sensibility of spectrometers. However, the configurations of the emission spectra measured at low temperature in Fig. 4 are completely different from those collected at room temperature shown in Fig. 5. The significant difference of the emission spectra between measured at room temperature and collected at low temperature shows the temperature-dependent luminescence of YBO_3: Sb^{3+}.

Moreover, the wavelength-selective excitation of YBO_3: Sb^{3+} luminescence is highlighted by comparing the emission spectrum upon 252 nm with 262 nm excitation, as displayed in the right hand side of Fig. 4. Fig. 4 demonstrates that the emission band peaked at about 410 nm is sensitive to the excitation of 168, 203, 218, 225 and 252 excitation while the emission band peaked at about 470 nm is sensitive to the excitation of 262 nm. The doublet structure could be discriminated clearly from the emission upon 168, 203, 218, 225, 252, and 262 nm excitation at 14 K. However,

it is difficult to determine the precise position of the doublet peaks in Fig. 5, besides the dominant one at about 400 nm. This difference indicates that the wavelength-selective excitation is also temperature-dependent.

From the doublet emission peaks in Fig. 4, we can conclude that all emission spectra presented in Figs. 3 and 5 should comprise two peaks as disclosed by their assymetric configuration. Thus, the emission spectra could be deconvoluted by fitting with two Gaussian Functions. Fig. 3 presents one of the fitted spectra upon the emission excited with 230 nm. The others are omitted.

Fig. 6 presents the excitation spectra of $(Y_{0.92}Sb_{0.08})BO_3$ by motoring the emission at 407/460 nm collected with Hitachi F-4500 spectrometer at room temperature, in which two absorption bands with peak at about 231/249 and 272/285 nm are observed, respectively. In contrast to the excitation bands upon 407 nm, the two excitation bands upon 460 nm red-shift about 18 nm and 13 nm, respectively.

The excitation spectra of $(Y_{0.92}Sb_{0.08})BO_3$ by motoring 407 and 460 nm measured on the NSRL instrument at room temperature are shown in Fig. 7. Quadruplet at 202, 211, 217 and 222 nm in the band region of 190–240 nm and a doublet at 250 and 264 nm

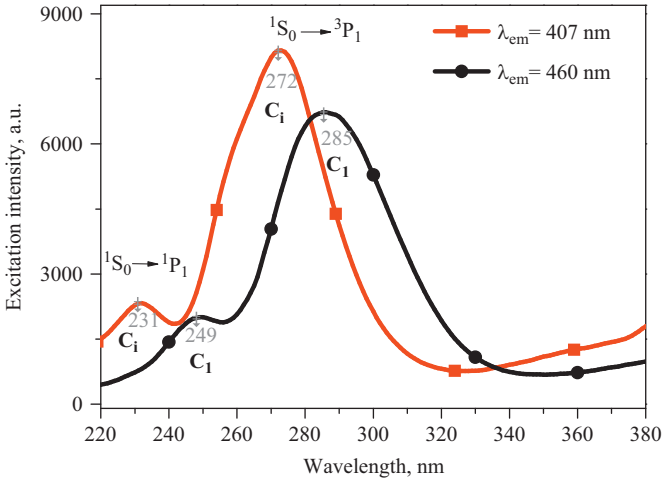

Fig. 6. The excitation spectra of $(Y_{0.92}Sb_{0.08})BO_3$ by motoring 407 and 460 nm emission collected with the Hitachi F-4500 spectrophotometer at room temperature.

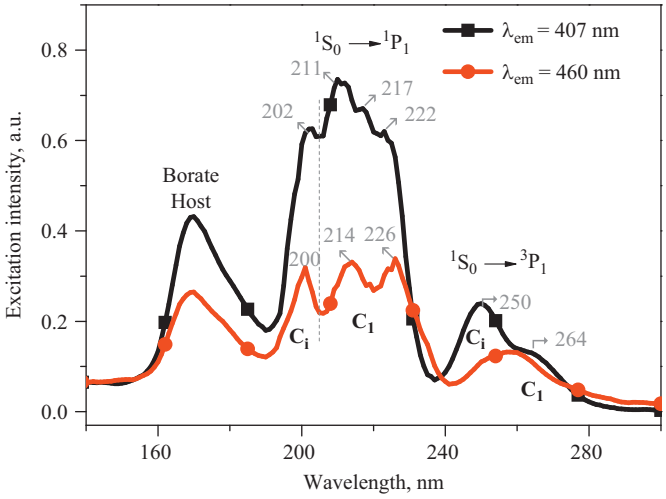

Fig. 7. The excitation spectra of $(Y_{0.92}Sb_{0.08})BO_3$ by motoring 407 and 460 nm emission measured on the NSRL synchrotron instrument at room temperature.

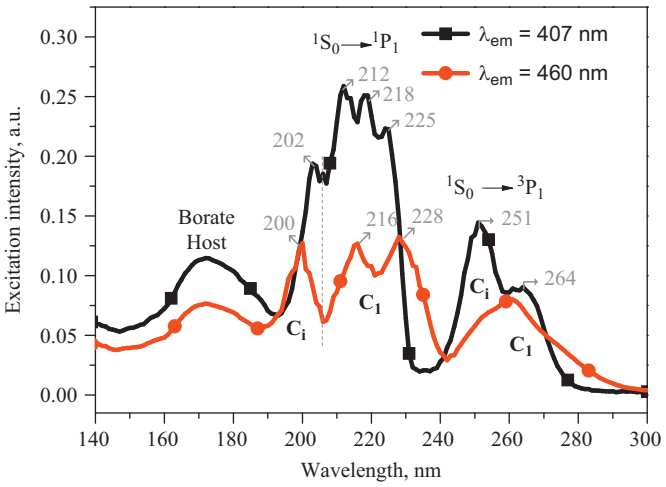

Fig. 8. The excitation spectra of $(Y_{0.92}Sb_{0.08})BO_3$ by motoring 407 and 460 nm emission measured on the BSRF synchrotron instrument at 14 K.

in the band region of 240–280 nm are observed in the excitation spectra upon 407 nm emission, while triplet peaks at 200, 214 and 226 nm in the band region of 190–240 nm and a singlet at 259 nm in the band region of 240–280 nm are presented by monitoring the emission of 460 nm. Besides configuration, the relative intensity of the excitation peaks differs from each other. Moreover, as far as the same temperature and the same monitoring wavelength conditions are considered, the excitation spectra in Fig. 6 differentiate significantly from those in Fig. 7.

Fig. 8 presents the excitation spectra by monitoring the emission at 407 or 460 nm measured on the BSRF instrument at 14 K. By comparing Fig. 7 with Fig. 8 at the same condition of monitoring wavelength, either 407 or 460 nm, the differences caused by temperature could be discriminated clearly. Firstly, the quadruple peaks at 202, 212, 218 and 225 nm in the band region of 190–240 nm upon 407 nm emission were clearly exhibited in Fig. 8, but they are obscure in Fig. 7, especially for the minor peak at 217 nm. Secondly, the splits of the triplet peaks at 200, 216 and 228 nm upon 460 nm emission at 14 K are much larger than those at room temperature. Thirdly, the doublet structure of the excitation band in the region of 240–280 nm at 14 K in Fig. 8 is more clearly displayed than in Fig. 7. These characters demonstrate the strongly temperature-dependent luminescence of YBO_3: Sb^{3+}.

4. Discussion

The ground state of Sb^{3+} for with [Xe]$5s^2$ electron configuration is $^1S_0$, whereas the excited state originating from $5s5p$ orbit gives rise to four levels, namely $^3P_0$, $^3P_1$, $^3P_2$, and $^1P_1$. The Mulliken notation for these levels become $^1A_{1g}$ (Γ_1^+) ground state and the three excited states, $^3T_{1u}$ (Γ_1^-, Γ_4^-, Γ_3^- and Γ_5^-), $^1T_{1u}$, and the perturbed exciton (Γ_4^-,)0.[4–13] The $^1T_{1u}$ and $^3T_{1u}$ excited states are well described by molecular orbits (MOs), a_{1g} and t_{1u} [4–13]. The transition $^1S_0 \rightarrow {}^1P_1$ is allowed, whose corresponding absorption band is denoted as the C band; the transition $^1S_0 \rightarrow {}^3P_1$ is partially allowed by spin–orbit coupling (A band); the transition $^1S_0 \rightarrow {}^3P_2$ is spin-forbidden (B band), but can be induced by lattice vibrations [4–13]. Correspondingly, the intensity of the B band usually is very weak. The transition $^1S_0 \rightarrow {}^3P_0$ is strictly forbidden for $\Delta J=0$, in which the total angular moment does not change.

In order to identify the appropriate electron transitions through the assignment of fine structures in excitation and emission spectra of Sb^{3+}, the site of Sb^{3+} in crystal lattice has

to be considered. By virtue of the same valence and similar ionic radius (Sb^{3+}: 0.76, and Y^{3+}: 0.89), as discussed above, the doped Sb^{3+} ions should occupy the sites Y^{3+} ions in the crystal lattice of YBO_3.

The nearest neighbor coordination environments of Y^{3+} in YBO_3 at the C_i and C_1 sites please refer to Fig. 6 in Ref. [24] and Fig. 1 in Ref. [25]. The eightfold Y^{3+} in C_i site is surrounded with $O_1(2)$, $O_2(2)$, $O_3(2)$ and $O_4(2)$, while the C_1 site is coordinated with $O_1(2)$, $O_2(2)$, $O_3(2)$, $O_4(1)$ and $O_5(1)$. The distances of the nearest-neighbor oxygen atoms for which the mean values at the C_1 and C_i sites are 235.6 and 238 pm, respectively [24,25]. According to the relationship between crystal field strength and ionic bond length, the parameter D_q was represented as follows [34]:

$$D_q = \frac{3ze^2r^4}{5R^5} \quad (1)$$

where D_q presents the crystal field stabilization energy (CFSE), R the bond length between a central ion and ligand ions, r the mean size of a central ion, and Z the charge of a central ion. A shorter bond length implies the stronger crystal field strength and the larger split of excited states. Correspondingly, the center of the gravity of the excited state is greatly reduced due to the nephelauxetic effect, and the long wavelength emission occurs for the larger Stoke shift. Therefore, a reasonable explanation for the emission spectra in Figs. 3–5 are all attributed to the $^3P_1 \rightarrow {}^1S_0$ transition of Sb^{3+}, the band peaked at about 410 nm is attributed to Sb^{3+} at the C_i site, and the band peaked at about 470 nm is attributed to Sb^{3+} at the C_1 site. Correspondingly, the excitation bands peaked at 231 and 272 nm upon 407 nm in Fig. 6 could be ascribed to the $^1S_0 \rightarrow {}^1P_1$ and $^1S_0 \rightarrow {}^3P_1$ transitions of Sb^{3+} at the C_i site; and the excitation bands peaked at 249 and 285 nm upon 460 nm in Fig. 6 could be assigned to the $^1S_0 \rightarrow {}^1P_1$ and $^1S_0 \rightarrow {}^3P_1$ transitions of Sb^{3+} at the C_1 site, respectively.

The diffuse-reflection spectra of YBO_3 and $(Y_{0.92}Sb_{0.08})BO_3$ are presented in Fig. 9. Compared with pure YBO_3 host, a broad absorption band in the range of 260–400 nm with an edge about 299 nm is observed in the diffuse-reflection spectrum of $(Y_{0.92}Sb_{0.08})BO_3$. This absorption band must originate from the Sb^{3+} ions, and the position of this band corresponds to the excitation band in the region of 240–340 nm in Fig. 6. So, the absorption is attributed to the transition of $^1S_0 \rightarrow {}^3P_1$ of Sb^{3+}. Restricted to the spectrometer, the absorption of high-energy levels which has been beyond the available range of the instrument is not observed from Fig. 9.

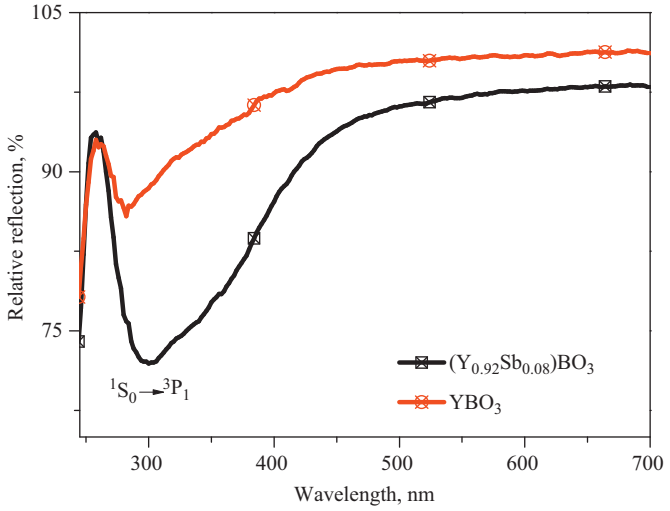

Fig. 9. The diffuse-reflection spectra of the pure host of YBO_3 and the phosphor of $(Y_{0.92}Sb_{0.08})BO_3$.

As revealed by the spectra of the Eu^{3+}/Tb^{3+} activated $(Y,Gd)BO_3$ system, the absorption band of borate host is independent of activators. Therefore, the excitation band in the region 150–190 nm with a peak at about 168 nm in Figs. 7 and 8 can be attributed to the absorption of the host band (HB) [17–19,35]. However, it is difficult to assign the fine peaks, i.e., the doublets at about 251 and 264 nm in the region of 240–280 nm upon 407 nm, the singlet at about 259 nm in the region of 240–280 nm upon 460 nm, the quadruplets at about 202, 211, 217 and 222 nm in the region of 190–240 nm upon 407 nm, and the triplets at about 200, 216 and 228 nm upon 460 nm, in Figs. 7 and 8. More interestingly, what does the mechanism correspond for the formation of the fine structures in excitation and how to explain them?

One possible explanation for the fine peaks is ascribed to the effect of site-selective excitation. The excitation band peaked at about 202 (200) and 251 nm could be attributed to the $^1S_0 \rightarrow {}^1P_1$ and $^1S_0 \rightarrow {}^3P_1$ transitions of the C_i site of Sb^{3+}, respectively. The others, including the triplets at 212, 218 and 225 nm upon 407 nm and the doublets at 216 and 228 nm upon 407 nm, in the region of 190–240 nm and the band peaked at about 262 nm in the region of 240–280 nm is attributed the $^1S_0 \rightarrow {}^1P_1$ and $^1S_0 \rightarrow {}^3P_1$ transitions of Sb^{3+} at the C_1 site, respectively, as marked in Figs. 7 and 8. Moreover, the triplets at 211, 217 and 222 nm could be interpreted as crystal field effect on the band splitting of C_1 for its trigonal symmetry, besides considering as electron vibration peaks. However, the presence of the $^1S_0 \rightarrow {}^3P_1$ absorption of Sb^{3+} at C_1 site (peaked at 264 nm) in the excitation by monitoring 407 nm of the $^3P_1 \rightarrow {}^1S_0$ emission of Sb^{3+} at C_i site cannot be interpreted by this mechanism, because electrons usually cannot transfer from a low energy state to a higher level automatically. If it happened, it must involve the phonon-coupling interaction. Moreover, the doublet splitting at 216 and 228 nm of C_1 site upon 460 nm emission could not be explained by the site-selective luminescence for its C_1 symmetry.

The site-selective luminescence of Bi^{3+}, which has the same ns^2 electronic configuration as Sb^{3+}, in the YBO_3 host was demonstrated by exciting/monitoring with different wavelengths at the low temperature in previous researches [36,37]. As for YBO_3: Bi^{3+}, the two emission bands peaked at 294 and 330 nm occur simultaneously by exciting C_i site with 247 nm; however, the emission band peaked at 294 nm does not show up by exciting C_1 site with 265 nm. Meanwhile, the excitation band peaked at 247 nm (C_i site) appears in the excitation spectra by monitoring both 330 (C_1 site) and 294 (C_i site) nm emissions, while the band peaked at 265 nm (C_1 site) does not occur to the excitation spectrum by monitoring 294 nm (C_i site) emission. The energy transfer between the symmetric and asymmetric sites of Bi^{3+} ions in YBO_3 was demonstrated at 22 K [36,37]. The results show that energy can be transferred from the $^1P_1$ and $^3P_1$ level of the C_i site to the $^1P_1$ and $^3P_1$ levels of the C_1 site, respectively, but can hardly be transferred from the $^1P_1$ (having less proportion) and $^3P_1$ (almost not) levels of the C_1 site to the $^1P_1$ and $^3P_1$ levels of the C_i site. For the same reason, if the doublets in Figs. 7 and 8 are caused by Sb^{3+} occupying different sites, the doublet emission peaks at 407 and 460 nm should occur simultaneously by exciting $^3P_1$ level of C_i site with 252 nm, and should only the band peaked at about 460 nm appear by exciting $^3P_1$ level of C_1 site with 262 nm; likewise, the dominant excitation band peaked at about 264 nm and the subordinate band peaked at 251 nm should both occur by monitoring the emission of C_1 site at 460 nm, and only the band peaked at 251 nm be observed by monitoring the emission of C_i site at 407 nm. Practically, the results shown in Figs. 7 and 8 are not consistent with these conclusions.

Another explanation is attributed to the superposition of the site-selective excitation and the dynamical electron–lattice interaction

(i.e. the Jahn–Teller effect) [6–13]. The Jahn–Teller split strongly depends on temperature. The relationship of the Jahn–Teller split with temperature is expressed by Jacobs and Oyama [38] as following equation:

$$\delta(T) = \delta(0)\sqrt{\coth\frac{\hbar\omega_{eff}}{2KT}} \quad (2)$$

where $\delta(0)$ is the Jahn–Teller splitting at $T=0$ K and ω_{eff} is an average frequency over all modes involved. According to the formula (2), the Jahn–Teller split should increase with temperature. The intensity of luminescence usually decreases while the full width at half maximum (FWHM) increases with temperature [6,8,9]. The middle of the triplet peaks at 217 nm in the band region of 190–240 nm in Figs. 7 and 8 clearly shows this character. Due to the linear and quadratic interaction with the ϵ_g and T_{2g} where lattice vibrations, the A band splits into doublet while the C band splits into triplet [10]. The doublet peaks at 252 and 264 nm occurring to the excitation spectrum 407 nm in Figs. 7 and 8 could be attributed to the adiabatic potential energy surface (APES) of the $^3P_1$ relaxed excited state which has two minima (the high energy level denoted as A_T and the low energy level denoted as A_x). The triplets at 211, 217 and 222 nm in the excitation spectra upon 407 nm and the doublets at 214 and 226 nm in the excitation spectra upon 460 nm in Figs. 7 and 8 could be ascribed to the Jahn–Teller effect on the $^1S_0 \rightarrow {}^1P_1$ transition of Sb^{3+} at C_i and C_1 sites, respectively.

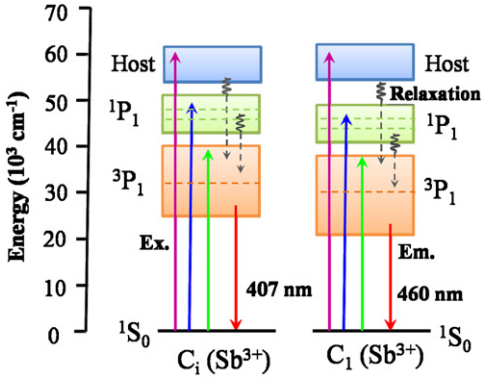

Fig. 10. The scheme of the energy levels of Sb^{3+} occupying at the sites of C_i and C_1 in the crystal lattice of YBO_3 and the processes of excitation (Ex.), emission (Em.) and nonradiative transition through electron relaxation.

Herewith, the energy levels of Sb^{3+} in YBO_3 including the borate host absorption and the processes of excitation, emission, and nonradiative transition through electron relaxation could be described as the scheme in Fig. 10, in which the dashed lines in energy level bands indicate the Jahn–Teller effect on the APES of $^1P_1$ and $^3P_1$ of Sb^{3+}.

To seek for another evidence to support the above conclusion about the multiple sites involved in the observed transitions, the phosphors activated by multiple Sb^{3+} concentrations were synthesized. Fig. 11 displays the emission and excitation spectra of $(Y_{1-x}Sb_x)BO_3$ (x=0, 0.001, 0.005 and 0.01) collected by using the F-4500 spectrometer at room temperature. With trace of Sb^{3+} doped into the YBO_3 host, the Sb^{3+} ions would preferentially occupy the C_i site of Y^{3+} for its high symmetry, but only a large amount doped Sb^{3+} will incorporate into the C_1 site for its low symmetry. From Fig. 11(a)–(d), so, we observe that the configuation of the emission and excitation spectra of the $(Y_{0.999}Sb_{0.001})BO_3$ are similar to those of $(Y_{0.995}Sb_{0.005})BO_3$ very much, no matter by exciting/ monitoring the C_i site with 252/ 400 nm or by exciting/monitoring the C_1 site with 270/460 nm. When the concentration of Sb^{3+} is increased to x=0.01, however,

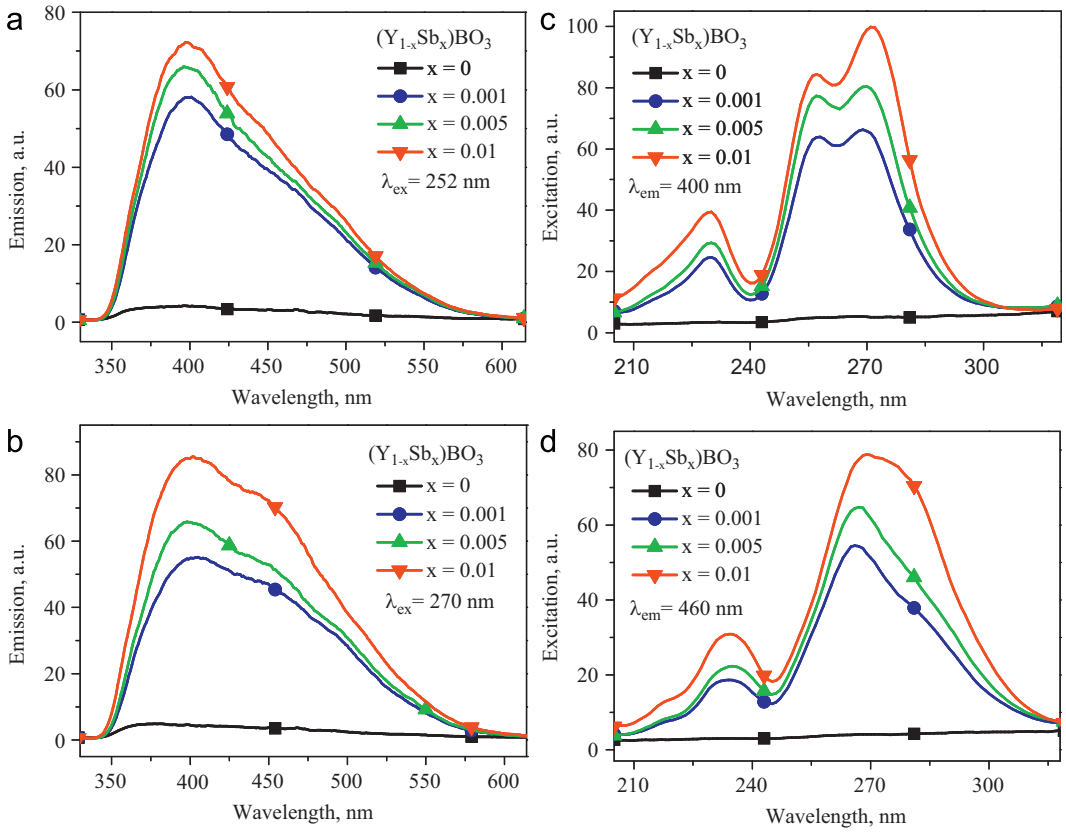

Fig. 11. The emission spectra of $(Y_{1-x}Sb_x)BO_3$ (x=0, 0.001, 0.005 and 0.01) excited with 252 and 270 nm for (a) and (b), respectively; and the excitation spectra by monitoring the emission at 400 and 460 nm for (c) and (d) respectively.

an extra emission and absorption of Sb^{3+} at C_1 site is observed obviously by comparing with the emission and absorption of Sb^{3+} at C_i site, especially from Fig. 11(b)–(d). The phenomena are consistent with expection.

By comparing with Bi^{3+} which has the same ns^2 electronic configuration with Sb^{3+}, we found that strong luminescence could be obtained by doping with very little Bi^{3+} (even trace of 0.02% M) into YBO_3 in our experiments. However, a larger amount of Sb^{3+} (the nominal optimal concentration is 8% M) should be doped so as to obtain efficient luminescence. This phenomenon suggests that electrons could transfer in a long range within different Bi^{3+} sites; however, it only happens in a short range for Sb^{3+}, which may be restrained by the strong electron–lattice coupling interaction between Sb^{3+} and YBO_3 host. A reasonable explanation for this difference is that the spin–orbit interaction of the heavy Bi^{3+} ion is much stronger than the electron–lattice interaction of Sb^{3+} ion [9].

To verify the availability of the above analyses, the fluorescence lifetime of Sb^{3+} emission was measured at room temperature. Fig. 12 presents the fluorescence decay curves by monitoring the emission at 400 and 460 nm, respectively, by exciting each with either 252 or 262 nm. The fluorescence decay spectra were fitted with exponential decay function as

$$I = A\exp\left(\frac{t}{\tau}\right) + C. \tag{3}$$

The fitted lifetime of τ for (a) (λ_{ex}=252 nm, λ_{em}=400 nm), (b) (λ_{ex}=252 nm, λ_{em}=460 nm), (c) (λ_{ex}=262 nm, λ_{em}=400 nm) and (d) (λ_{ex}=262 nm, λ_{em}=460 nm) are 0.00991, 0.01028, 0.01068 and 0.01102 ms, respectively. The lifetime of a forbidden transition usually is millisecond. So, the microsecond lifetime indicates that the emission must come from an allowed transition, which supports the above attribution of the emission band to the $^3P_1 \rightarrow {}^1S_0$ of Sb^{3+}. Nevertheless, the lifetime of an allowed transition from the p to the s orbit through electric dipole interaction usually is nano second. A reasonable explanation for the microsecond lifetime may be caused by energy transfer among different sites of Sb^{3+} and phonon–electron coupling, as consisting with the above analysis of the electron–lattice interaction on the luminescence of YBO_3: Sb^{3+}. Therefore, the attribution of the doublet emission in Figs. 3–5 to the $^3P_1 \rightarrow {}^1S_0$ transition and the assignment of the doublet excitation in the band region of 240–280 nm to the $^1S_0 \rightarrow {}^3P_1$ transition in Figs. 7 and 8 are reasonable. Restricted to experimental instruments, the lifetime of luminescence as corresponding to the excitation at quadruple peaks about 202, 211, 217 and 222 nm in the region of 190–240 nm was not carried out.

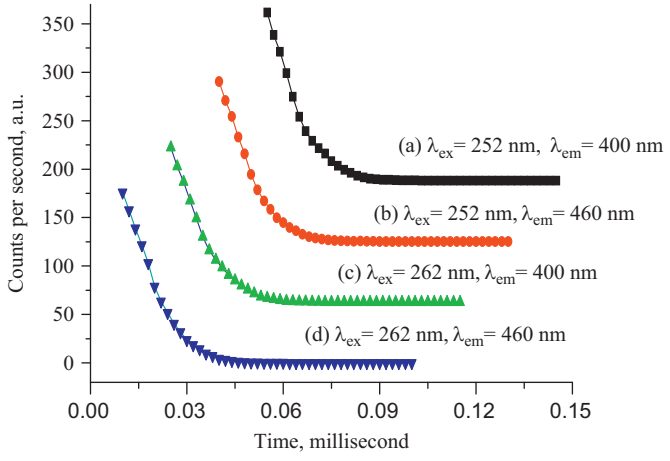

Fig. 12. The lifetime of YBO_3: Sb^{3+} upon 400 and 460 nm emission by respectively exciting with either 252 or 262 nm.

Finally, the parameters about the Jahn–Teller effect were calculated by using the molecular-orbital approximation. The formulae about the sum of the Coulomb energy and the energy difference between the ground state and excited state F_0, the spin–orbit coupling constant ζ, the exchange energy G, and the dipole strength ratio of the C band to the A band R_{th}, are given by Fukuda and Sugano as follows [39,40]:

$$F_0 = \tfrac{1}{4}\zeta + W_0, \quad \text{where } W_0 = \tfrac{1}{2}(W_A + W_C) \tag{4}$$

$$\zeta = \tfrac{2}{3}(W_B - W_0) + \tfrac{1}{3}[6(W_B - W_0)^2 - (W_B - W_0)^2]^{1/2} \tag{5}$$

$$G = \tfrac{3}{4}\zeta - (W_B - W_0) \tag{6}$$

$$R_{th} = \frac{(W_C - W_A) + \overline{W}}{(W_C - W_A) - \overline{W}}, \quad \text{where } \overline{W} = 2\zeta - 2(W_B - W_0) \tag{7}$$

W_A, W_B and W_C correspond to the peak wavelength of A, B and C band, respectively.

The strongest absorption at about 251 and 212 nm were considered as the mean value of C_1 and C_i site on the position of A and B bands, respectively. However, the B band which originates from a spin-forbidden transition of $^1S_0 \rightarrow {}^3P_2$ induced by lattice vibrations was not clearly observed. If happened, it should be close to the foot mountain of C band in the right hand. So, it was estimated to be 235 nm. The calculated values of the parameters F_0, ζ, G, and R_{th} according to Eqs. (4)–(7) with the available parameters of free Sb^{3+} is presented in Table 1.

5. Conclusions

In summary, the photoluminescence of YBO_3: Sb^{3+} was investigated systematically under the VUV and UV excitation at variant temperature conditions. The site-selective luminescence of YBO_3: Sb^{3+} was revealed by exciting/monitoring with different wavelengths and confirmed by the YBO_3 activated with multiple Sb^{3+} concentrations. More importantly, the superposition of the Jahn–Teller effect and sites effect on the luminescence of YBO_3: Sb^{3+} was discriminated from the hyperfine structure in excitation spectra which were measured on the synchrotron radiation instrument at 14 K low temperature. Although Bi^{3+} and Sb^{3+} has the same ns^2 electronic configuration, the luminescence of

Table 1
Values of the parameters F_0, ζ, G, and R_{th} (eV).

	W_C	W_B	W_A	F_0	ζ	G	R_{th}	
Free Sb^{3+}	11.90	9.00	8.27	10.25	0.67	1.59	57.35	Ref. [21]
YBO_3: Sb^{3+}	5.9161	5.2870	4.9695	5.5117	0.2755	0.3625	21.5584	300 K
	5.8603	5.2421	4.9301	5.4629	0.2708	0.3562	21.5583	22 K

Sb^{3+} in YBO_3 host distinguish from that of Bi^{3+} significantly. The strong electron–lattice interaction between Sb^{3+} and YBO_3 host will affect the energy transfer from Sb^{3+} to other activators, if it were served as a sensitizer. Accordingly, appropriate measures, such as the replacement of Y^{3+} by a heavy Lu^{3+} one, should be taken to suppress the electron–lattice interaction in order to improve luminescence. More researches are undertaking.

Acknowledgments

The authors acknowledge the financial support from the National High-Tech R&D Program of China (863 program) for semiconductor lighting application and demonstration of "Ten cities with all LED lamps" (ss2013AA030114), the National Natural Science Foundation of China (Nos. 51002043, 51172086, 51272081, and 61076040), the Science Foundation for Excellent Young Scholars of the Ministry of Education of China (No. 20090111120001), the Science and Technology Program of Anhui Province (No. 12010202004), the China Postdoctoral Science Foundation (Nos. 20090450802 and 2012T50568), the Fundamental Research Funds for the Central Universities (2012HGQC0033), and the Student Innovation Training Program of Hefei University of Technology (Nos. 2012CXCY071 and 2012CXCY044).

References

[1] S. Nigam, V. Sudarsan, R.K. Vatsa, Opt. Mater. 33 (2011) 558–562.
[2] F. Wen, W. Li, Z. Liu, T. Kim, K. Yoo, S. Shin, J.H. Moon, J.H. Kim, Solid State Commun. 133 (2005) 417–420.
[3] H.C. Jung, J.Y. Park, G.S.R. Raju, B.C. Choi, J.H. Jeong, B.K. Moon, J. Am. Ceram. Soc. 94 (2011) 551–555.
[4] G. Blasse, B.C. Grabmaier, Luminescent Materials, Springer Press, Berlin, 1994, p. 55, 115.
[5] S. Shionoya, W.M. Yen, Phosphor Handbook, CRC Press, Boca Raton, 1998, p. 393.
[6] E.W.J.L. Oomen, G.J. Dirksen, W.M.A. Smit, G. Blasse, J. Phys. C: Solid State Phys. 20 (1987) 1161–1171.
[7] L.I.V. Steensel, G. Blasse, J. Alloys Compd. 232 (1996) 60–62.
[8] E.W.J.L. Oomen, R.C.M. Peeters, W.M.A. Smit, G. Blasse, J. Solid State Chem. 73 (1988) 151–159.
[9] E.W.J.L. Oomen, W.M.A. Smit, G. Blasse, J. Phys. C: Solid State Phys. 19 (1986) 3263.
[10] A. Fukuda, Phys. Rev. B 1 (1970) 4161–4178.
[11] Y. Toyozawa, M. Inoue, J. Phys. Soc. Jpn. 21 (1966) 1663–1679.
[12] J. Grafmeyer, J.C. Bourcet, J. Janin, J.P. Denis, J. Loriers, J. Lumin. 11 (1976) 369–380.
[13] R. Reisfeld, L. Boehm, B. Barnett, J. Solid State Chem. 15 (1975) 140–150.
[14] P.J. Boyle, Adv. Space Res. 42 (2008) 409–416.
[15] J.A.M. Lopes, J.M.F. dos Santos, R.E. Morgado, C.A.N. Conde, IEEE Trans. Nucl. Sci. 48 (2001) 312–319.
[16] C.M.B. Monteiro, R.E. Morgado, J.M.F. Santos, C.A.N. Conde, Nucl. Instrum. Methods Phys. Res. A 522 (2004) 407–412.
[17] L. Chen, Y. Yang, Y. Yang, J. Huang, J. Shi, S. Chen, J. Phys. D: Appl. Phys. 42 (2009) 215104-3.
[18] L. Chen, G. Yang, J. Liu, X. Shu, Y. Jiang, G. Zhang, J. Appl. Phys. 105 (2009) 013513-013513.
[19] L. Chen, Y. Jiang, G. Yang, G. Zhang, X. Xin, D. Kong, J. Rare Earths 27 (2009) 312–315.
[20] E.W.J.L. Oomen, L.C.G. van Gorkom, W.M.A. Smit, G. Blasse, J. Solid State Chem. 65 (1986) 156–167.
[21] N. Yamashita, J. Phys. Soc. Jpn. 35 (1973) 1089–1097.
[22] Y. Tao, Y. Huang, Z. Gao, H. Zhuang, A. Zhou, Y. Tan, D. Li, S. Sun, J. Synchrotron Rad. 16 (2009) 857–863.
[23] G. Chadeyron, M. El-Ghozzi, R. Mahiou, A. Arbus, J.C. Cousseins, J. Solid State Chem. 128 (1997) 261–266.
[24] J. Lin, D. Sheptyakov, Y. Wang, P. Allenspach, Chem. Mater. 16 (2004) 2418–2424.
[25] G. Jia, P.A. Tanner, C.K. Duan, J. Dexpert-Ghys, J. Phys. Chem. C 114 (2010) 2769–2775.
[26] E.M. Levin, R.S. Roth, J.B. Martin, Am. Mineral. 46 (1961) 1030–1055.
[27] R.E. Newnham, M.J. Redman, R.P. Santoro, J. Am. Ceram. Soc. 46 (1963) 253–256.
[28] W.F. Bradley, D.L. Graf, R.S. Roth, Acta Crystallogr. 20 (1966) 283–287.
[29] H.M. Kriz, P.J. Bray, J. Chem. Phys. 51 (1969) 3624–3625.
[30] R. Bohlhoff, H.U. Bambauer, W.Z. Hoffman, Kristallografiya 133 (1971) 386–395.
[31] J.H. Denning, S.D. Ross, Spectrochim. Acta A 28 (1972) 1775–1785.
[32] E. Antic-Fidancev, J. Aride, J. Chaminade, M. Lemaitre-Blaise, P. Porcher, J. Solid State Chem. 97 (1992) 74–81.
[33] M. Ren, J.H. Lin, Y. Dong, L.Q. Yang, M.Z. Su, Chem. Mater. 11 (1999) 1576–1580.
[34] X. Zhang, J. Zhang, J. Huang, X. Tang, M. Gong, J. Lumin. 130 (2010) 554–559.
[35] C.H. Kim, I.E. Kwon, C.H. Park, Y.J. Hwang, H.S. Bae, B.Y. Yu, C.H. Pyun, G.Y. Hong, J. Alloys Compd. 311 (2000) 33–39.
[36] L. Chen, H. Zheng, J. Cheng, P. Song, J. Lumin. 128 (2008) 2027–2030.
[37] L. Chen, Y. Jiang, G.B. Zhang, C. Wu, G.T. Yang, C. Wang, G.H. Li, Chin. Phys. Lett. 25 (2008) 1884–1887.
[38] P.W.M. Jacobs, K. Oyama, J. Phys. C: Solid State Phys. 8 (1975) 851–864.
[39] A. Fukuda, K. Inohara, R. Onaka, J. Phys. Soc. Jpn. 19 (1964) 1274–1280.
[40] S. Sugano, J. Chem. Phys. 36 (1962) 122–123.